Failure Mode Analysis of Photonic Components on InP Using Low-Coherence Reflectometry: Case of Burned DBR Lasers

C. Plouzennec, Y. Gottesman, E. V. K. Rao, H. Sillard, A. Plais, and J. Jacquet

***Abstract*—The high potential of optical low-coherence refletometry to investigate the failure mode of InP-based optical devices is demonstrated here by considering two examples of burned (under high optical output power and operating temperature) distributed Bragg reflector lasers on InP. In addition to monitoring reflections in the conventional reflection mode, these two-section devices (active amplifier section and passive Bragg section) are further examined using other in-situ facilities such as the transmission and edge electroluminescence measurements. A comprehensive analysis of these data in comparison to a reference device permitted the following: 1) the spatial localization of burning induced damage only in the amplifier section; 2) some relevant information on the nature of defects in the damaged region, such as their nonradiative character and structural modifications in multiquantum wells, which tentatively are attributed to the occurrence of intermixing between well and barrier layers.**

***Index Terms*—Bragg grating, burning test, distributed Bragg reflector laser, edge electroluminescence, failure mode, integrated optics, low-coherence reflectometry.**

I. Introduction

With the advent of high-speed optical fiber communications, tremendous progress has been accomplished in recent years on the development of photonic integration technologies on InP for wavelength-division multiplexing (WDM) applications. The inherent high complexity of these integration technologies also initiated, in parallel, a good deal of research to improve device yield at reduced cost and most importantly to achieve highly reliable and reproducible performances. This obviously necessitated a thorough understanding of the device and/or circuit failure modes under exaggerated operation conditions to test the robustness of the material and also the processing technologies. As a result, a variety of testing procedures, such as burning and aging, are currently experimented with using stress conditions (optical, electrical, and thermal) far beyond those required for normal device operation. In this context, we propose and demonstrate here that the conventional optical low-coherence reflectometry (OLCR) analysis, when coupled to other deliberately incorporated in-situ facilities such as transmission and edge-electroluminescence (EEL) measurements, can greatly help to investigate the device failure mode mechanisms. More precisely, we show here that such a combination alone permits a nondestructive in-situ evaluation of the optical (by OLCR mode measurements) and also the optoelectronic quality (by EEL mode measurements) of waveguide cavities required for investigating the failure mode of distributed Bragg reflector (DBR) lasers.

Manuscript received January 31, 2003; revised September 17, 2003. This work was supported by the Région Ile de France under SESAME Project 1377 and by the Conseil Générale de l'Essone.

C. Plouzennec is with CNRS-LPN, 91460 Marcoussis, France, and Valeo, 89107 Sens, France.

Y. Gottesman is with CNRS-LPN, 91460 Marcoussis, France, and Institute National de Telecommunications, 91011 Evry, France.

E. V. K. Rao is with CNRS-LPN, 91460 Marcoussis, France.

H. Sillard, A. Plais, and J. Jacquet are with ALCATEL/OPTO+, 91460 Marcoussis, France.

Digital Object Identifier 10.1109/JLT.2003.821757

II. Experimental

To demonstrate the high potential of OLCR in the field of optical device failure mode analysis (FMA), we consider here the case of monolithically integrated and identically processed DBR lasers on InP substrate. These two-section devices, as described in detail in [1], are composed of an amplifier section containing an InGaAsP-based multiple quantum well structure (active waveguide) and a Bragg section with a bulk InGaAsP waveguide realized in a separate growth sequence. The completion of whole device, in addition to Bragg grating inscription, necessitated at least four different growth sequences and intermediate etchings. Such as-processed devices with antireflection (AR) coatings at the facets exhibited remarkably low laser threshold ($I_{\rm th} \sim 8$ mA) and a reasonably wide wavelength tuning range ($\sim$12 and $\sim$15 nm). However, after a burning test carried out under voluntarily exaggerated conditions (ten times the threshold current ($I_{\rm th}$) on the active section, twice the tuning current on the Bragg section and an operating temperature close to 100 °C), two such devices (DBR #1 and DBR #2) failed to function despite no visible mechanical damage as confirmed from optical microscope examination. These degraded devices together with an as-processed reference laser (DBR #R) are precisely considered here for failure mode analysis using OLCR and other deliberately incorporated in-situ facilities, as described below.

The OLCR setup shown here as Fig. 1 and described in detail in our earlier reports [2]–[4] is basically a Michelson interferometer equipped with a broadband (a spectral half-width of $\sim$55 nm) low-coherent light probe centered at $\sim$ 1.56 μm. The device under test (DUT) is coupled to one of the interferometer arms using a single-mode fiber (SMF) while the other contains a movable reference mirror that can scan a wide range of optical paths to detect refractive index discontinuities as low as 10^{-5} in the test device. When the optical path length of a reflecting

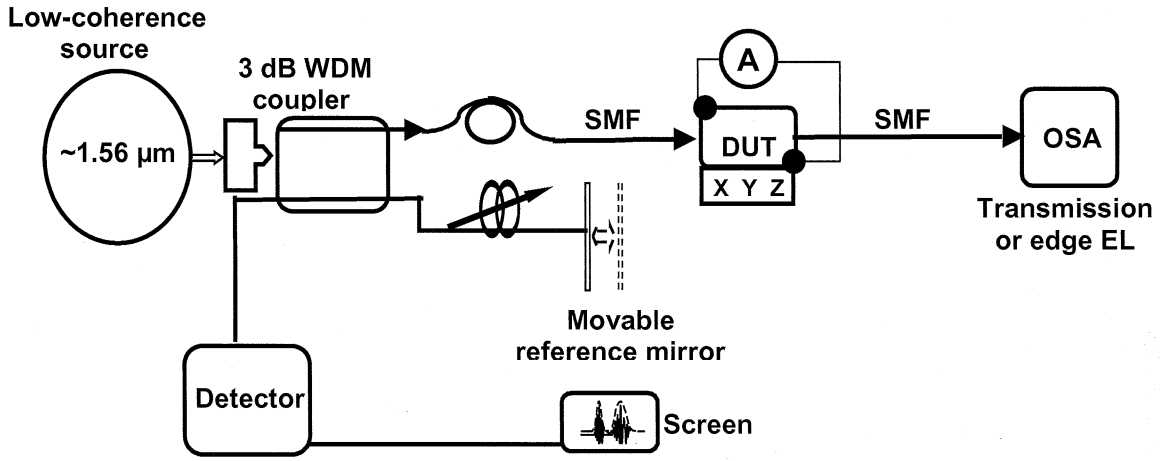

Fig. 1. Simplified block diagram of a conventional OLCR setup and the voluntarily incorporated in-situ EEL mode facility to perform spectral analysis. Here, the DUT is lodged on a sample holder with fine x, y, and z movements and is provided with a facility (A) to inject carriers into the device. The coupling of light into and out of the DUT is accomplished using lensed SMFs and the spectra of transmitted probe light and/or EEL are recorded by connecting the output fiber to an OSA. The reflectograms are recorded in reflection mode by scanning the reference mirror, and the interference is detected by a detector designed for fringe envelop detection.

center (or a refractive index discontinuity) in the test device becomes equal to that in the reference arm, an intense interference signal corresponding to its location in the waveguide cavity will be detected (envelop detection) over a distance only dependent on the source coherence length. The OLCR measurements are carried out under conditions of single-mode propagation by coupling the probe light into the DUT waveguide cavity using a lensed SMF (see Fig. 1). The abscissa of the reflectogram thus recorded corresponds to the optical path in air, while the ordinate represents the return losses (given as $\mathbf{10}\log(\mathbf{P_r}/\mathbf{P_i})$) in dB, where $\mathbf{P_r}$ and $\mathbf{P_i}$ represent respectively the reflected and incident light intensities) experienced at a *localized reflection*. Such data can be exploited to qualify the device optical quality (propagation losses, scattering induced losses, etc.) and further help to localize defects, if any, present in the cavity. In the case of a Bragg grating, as recently shown in [3], the probe light experiences spatially *distributed reflections* and the resulting reflectogram permits to extract the Bragg parameters. In all cases, the abscissa of a reflectogram can be converted into distance in the sample from knowledge of the device physical length and the effective group refractive index.

Also, since these devices contained a p-n junction in each section whose injection properties are critical to their performance, we have voluntarily incorporated additional in-situ facilities in the existing OLCR setup to further qualify the optoelectronic quality (nonradiative centers, electroluminescence spectra, etc.) of the device cavity. These facilities greatly helped to record simultaneously (in addition to conventional OLCR measurements in reflection mode) the transmitted probe light spectra [3], [4] and, most importantly, the EEL spectra under controlled injection of free carriers in the device using a lensed SMF and an optical spectrum analyzer (OSA) (see Fig. 1). Thus, this upgraded OLCR, in contrast to a conventional setup, gave access to monitor in-situ the optical and also the optoelectronic quality of the device cavities to assess on the influence of burning-induced damage in DBR lasers.

III. Results and Discussion

Unlike in the case of a discrete Fabry–Perot type laser, the failure of a monolithically integrated two-section DBR laser can originate from different sources (higher threshold and/or poor tuning). For example, the damage-induced defects can be spatially localized either in the amplifier section or in the Bragg section and possibly also in both sections. Furthermore, depending on their specific nature, the defects could be either electrically active (nonradiative centers) or optically active (reflection, scattering, etc.) and/or active in both ways. This means a study on the failure mode analysis of DBR lasers must necessarily gather relevant information on the optical and also the optoelectronic quality of the device in each section separately. To this end, we first employed OLCR in its conventional reflection mode to identify modifications in the optical quality of device cavities by recording reflectograms. This consisted of detecting and spatially localizing newly introduced reflection centers in the device waveguide cavities including modifications, if any, in the characteristics of Bragg grating. Later, the setup is operated in EEL mode by injecting carriers in the amplifier section to record EL spectra at either end of each device: amplifier end or Bragg end. These measurements are carried out to monitor the optoelectronic quality of device cavities and also to learn their light transmission properties subsequent to burning test.

A. OLCR in Reflection Mode

We have reported in a recent paper that OLCR measurements, when performed simultaneously in reflection and transmission modes, permit evaluation of the principal characteristics (coupling coefficient $\boldsymbol{\kappa}$ and Bragg wavelength $\boldsymbol{\lambda_B}$) of a Bragg grating in monolithically integrated DBR lasers on InP [3]. In that study, the reflectograms computed using transfer-matrix method (TMM) have been compared with those recorded by coupling the OLCR probe successively on either ends of the device (amplifier end and Bragg end). With that knowledge, we

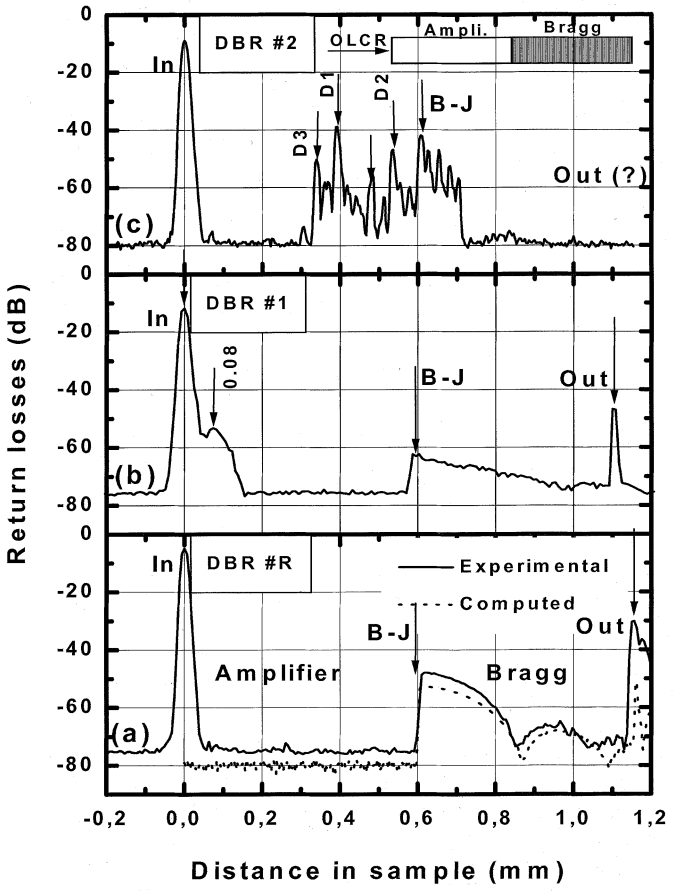

Fig. 2. Comparison of reflectograms belonging to the reference [(a) DBR #R] and burned [(b): DBR #1; (c): DBR #2] DBR lasers recorded in the reflection mode by coupling the OLCR probe at the amplifier end [see inset of (c)]. The reflectograms of identically processed reference device DBR #R [experimental and computed: (a)] taken from [3] are included here to facilitate the identification of burning induced modifications.

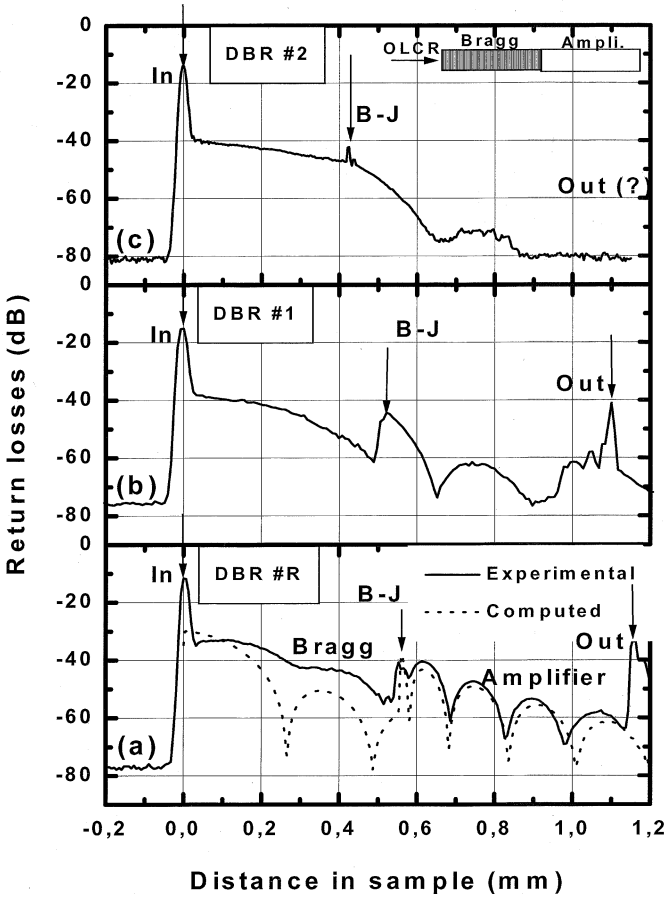

Fig. 3. Comparison of reflectograms belonging to the reference [(a): DBR #R] and burned [(b): DBR #1; (c): DBR #2] DBR lasers recorded in the reflection mode by coupling the OLCR probe at the Bragg end [see inset of (c)]. As in Fig. 2, the experimental and simulated reflectograms of DBR #R (a) taken from [3] are also included to facilitate comparison.

now focus our attention on the evolution of reflectograms in the two burned DBR lasers (DBR #1 and DBR #2) in comparison to the reference device (DBR #R). Figs. 2 and 3, respectively, show such data recorded successively by coupling the OLCR probe at the amplifier end [Fig. 2(a)]: DBR #R); Fig. 2(b): DBR #1; and Fig. 2(c): DBR #2); and the Bragg end [Fig. 3(a)]: DBR #R; Fig. 3(b): DBR #1; and Fig. 3(c): DBR #2). As seen in these figures, the locations of principal reflecting planes are labeled on each reflectogram as "in" and "out" for the device facets and "B-J" (butt-joint) for the transition region between amplifier and Bragg sections. Also, the examples of computed reflectograms belonging to the reference laser (DBR #R) taken from [3] are shown here for comparison [see Figs. 2(a) and 3(a)].

Turning to Fig. 2, the following two important modifications in the reflectograms of the burned devices can be identified in comparison to DBR #R. First, the emergence of a well-defined reflection peak in the reflectogram of DBR #1 located close to the input end ($\sim$ 80 μm) of its amplifier section [see Fig. 2(b)]. Second, the presence of multiple reflections spread on either side of the transition region (B-J) of DBR #2 [see Fig. 2(c)] and a nearly absent reflection peak at the out facet suggest a poor transmission across the device. Although one can at present assess on the spatial localization of burning-induced damage in DBR #1 [from the presence of additional reflection in Fig. 2(b)], the damage localization in DBR #2 is, however, not as straightforward, as will be evident from the data shown in Fig. 3 (recorded with OLCR probe at Bragg end). Indeed, from this figure, one can easily notice that the portion of the reflectogram corresponding to the Bragg section of all devices is comparable [compare Fig. 3(a)–(c)] excepting few minor variations in reflection amplitudes. This striking observation points out a few interesting additional features concerning the damage in DBR #2. First, the Bragg section of this device is free of damage. That is, the damage-induced defects seem to be spatially distributed alone in the amplifier section. Second, the multiple reflections detected on either side of B-J in DBR #2 [refer to Fig. 2(c)] are most likely a consequence of probe light round-trips within the damaged portion of the amplifier section, which ultimately led to poor transmission across the device. After these early conclusions on the presence of damage in the cavities of burned devices only accessible to measurements in OLCR mode, we further monitored in-situ their optoelectronic quality in EEL mode to learn more about the nature of damage and, if possible, its origin as well.

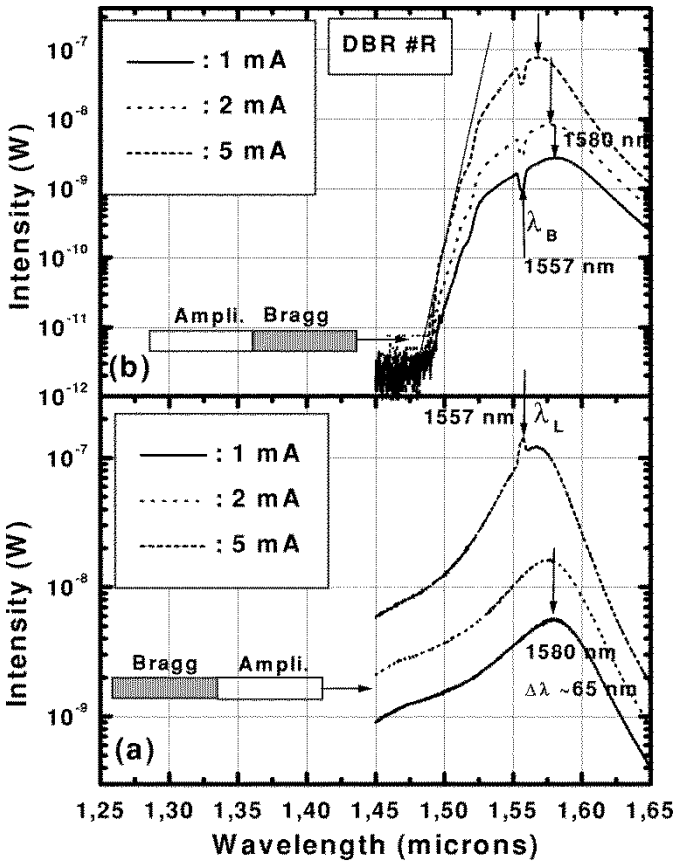

Fig. 4. Evolution of EEL spectra recorded at the amplifier end [Fig. 2(a)] and Bragg end [Fig. 2(b)] for different injection currents in the amplifier section of the reference laser (DBR #R). The thin straight line intersecting the wavelength axis in (b) denotes the transmission threshold (i.e., the fundamental absorption) in the Bragg section. Note the close correspondence between λ_L [in (a)] and λ_B [in (b)], which clearly denote the optimal functioning of a DBR laser device.

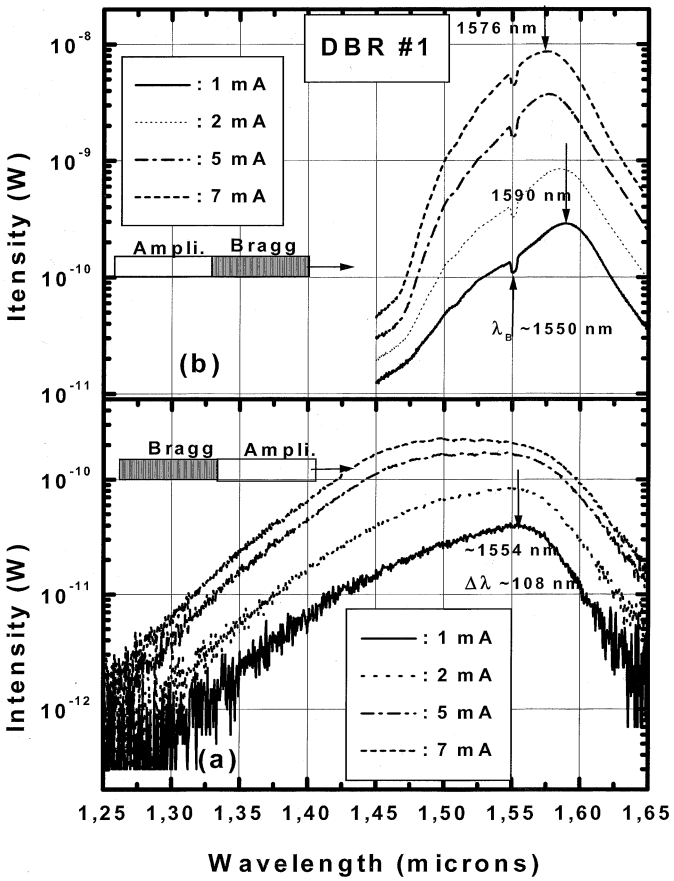

Fig. 5. The EEL spectra recorded at the the amplifier end (a) and Bragg end (b) of the burned laser (DBR #1) for different injection currents in the amplifier section. The significant spectral modifications (peak position, half-width, and spectral distribution) seen in (a) as compared to (b) are worth noting.

B. EEL Mode

As mentioned before, these measurements are carried out by injecting carriers in the amplifier section and recording the EEL spectra on either end of the device (amplifier end and Bragg end). Here, our objectives are threefold: first to assess the quality of p-n junction injection in the amplifier section; second to monitor the EL spectral modifications in the burned devices; and third to investigate the light transmission properties across the Bragg section in near-device operating conditions. All these measurements are of course carried out in comparison to the reference laser, whose data can be seen from Fig. 4. We compared in this figure the EEL spectra recorded at either end of the reference device [Fig. 4(a): amplifier end and Fig. 4(b): Bragg end] for different levels of current injection in the amplifier section. As expected, one can notice in Fig. 4(a) all known characteristic evolutions in the spectra from the amplifier end with increasing injection current [5]. These are, for example, a blue-shift of the peak due to band filling, narrowing of spectral linewidth due to increased amplification in the device cavity, and further the emergence of a sharp peak indicating the commencement of laser emission (λ_L). Likewise, the EEL spectra from the Bragg end [see Fig. 4(b)] exhibit a sharp and well-defined drop in transmitted light intensity caused by a higher reflectivity at the Bragg wavelength (λ_B). This wavelength precisely corresponds to the laser emission confirming the high λ-selectivity of Bragg grating. Other interesting features of these EEL spectra worth noting are as follows.

1) For a fixed injection current, the spectra recorded from either end show no peak shift, revealing thereby and as expected a complete transmission across the Bragg section.
2) Also, a marked threshold in transmission [$\sim$ 1.47 μm, see Fig. 4(b)] corresponding to the bandgap of quaternary material in the Bragg guide.
3) The EL intensity ratio of the spectra from either end is nearly close to the value one would expect for transmission through AR coated facets.

1) EEL Mode Analysis of DBR #1: In light of the above considerations, which establish a framework of reference to analyze EEL spectra, let us turn to Fig. 5, which depicts data belonging to the burned device DBR #1 [Fig. 5(a): amplifier end and Fig. 5(b): Bragg-end]. Let us first recall here that the reflectogram of this device revealed a well-defined reflection peak located around $\sim$ 80 μm near the amplifier end [see Fig. 2(b)]. Now, a simple comparison with the EEL data of reference device (shown in Fig. 4) highlights several important spectral modifications in DBR #1 that can be summarized as follows.

1) The abnormally large half-width for the 1-mA spectrum from amplifier end [$\sim$ 108 nm in Fig. 5(a) compared to $\sim$65 nm for DBR #R; see Fig. 4(a)], which essentially is characterized by a preferential broadening on the high-energy side.
2) A dramatically reduced EL intensity for all spectra from the amplifier end compared to the reference device irrespective of the injected current value.
3) A surprisingly higher EL intensity for all spectra from the Bragg end [Fig. 5(b)] as compared to their counterparts [Fig. 5(a)] from the amplifier end (far more than ten times).
4) Unlike in the reference device, a totally unexpected blue-shift of the EL peaks from the amplifier end compared to their counterparts from the Bragg end [$\sim$1554 nm in Fig. 5(a) compared to $\sim$1590 nm in Fig. 5(b)].

A satisfactory explanation for all of the above observations, which alone are accessible to EEL mode analysis, can be provided by assuming few specific properties for the damaged region in DBR #1. In close agreement with observation 2), the dramatic reduction in EEL intensity in DBR #1 can be attributed to the presence of structural and/or line defects (dislocations) in the damaged region, which would act as nonradiative centers in the neighborhood of the amplifier exit end. This means, under a uniform carrier injection, only a limited portion of the amplifier section closer to the exiting end is alone affected by a severe nonradiative recombination while the rest of it (up to the B-J) remained intact, i.e., not affected by nonradiative recombination. Such an assumption, in total agreement with observation 3), further comforts higher EL intensities for the spectra recorded from the Bragg end. Moreover, their spectral distributions would be closer to those recorded from the reference device [compare spectra of Figs. 5(b) and 4(b)]. On the other hand, observations 1) and 4), which dictate a higher spectral half-width and a marked blue-shift of the EL peaks, permit one to predict the occurrence of a partial intermixing between well and barrier layers in the damaged portion of the amplifier. Considering the low diffusivity of the matrix elements (in particular the group V atoms), we rather suspect here a significant temperature rise in the laser cavity and/or an abnormally enhanced defect induced interdiffusion to be at the origin of observations 1) and 4). In view of these remarks, we now analyze the characteristics of the burning-induced damage in device DBR #2 as deduced from the EEL mode data.

2) EEL Mode Analysis of DBR #2: We have seen before that the OLCR data on DBR #2, unlike in the case of DBR #1, revealed the presence of multiple reflection peaks all originating in the amplifier section. Also, we have further remarked that such reflections might possibly lead to poor transmission across the whole device as judged from the absence of a reflection at the device out-facet. (This property is further confirmed experimentally by performing direct transmission measurements using OLCR probe light as source.) Consequently, we have restrained the EEL mode analysis to the spectra from the amplifier end but voluntarily extended them further to find out the prominence of damage-induced reflections limiting transmission across the device. The latter procedure, as detailed in our earlier reports [6], [7], consisted of applying the fast Fourier transformation (FFT) treatment to the EEL spectra recorded at a high spectral resolution to identify the dominant resonant cavities in the guiding structure.

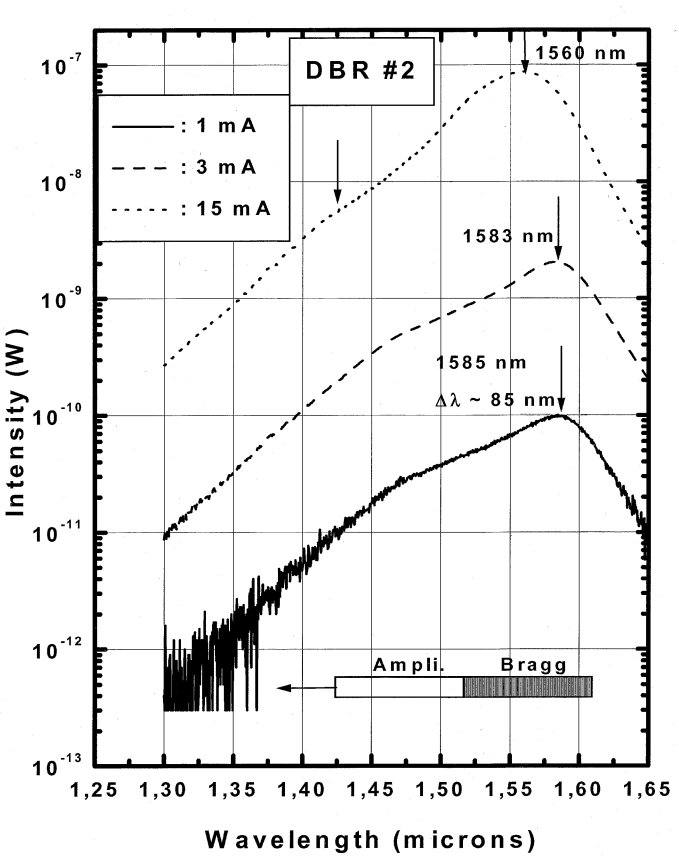

Fig. 6. EEL spectra recorded at the amplifier end of the burned device DBR #2 for different injection currents in the amplifier section. Note the reduced overall EL intensity and increased spectral half-width compared to the reference laser [Fig. 4(a)].

Let us now consider the data shown in Fig. 6, which depicts the EEL spectra recorded from the amplifier end of DBR #2 at different injection currents. Even though this device exhibits a slightly higher overall EEL intensity compared to DBR #1 [compare with Fig. 5(a)], it is evident from Fig. 6 that its amplifier section also suffers from nonradiative recombination since no lasing action is observed even at an injection current as high as 15 mA [compared to 5 mA in the reference device; see Fig. 4(a)]. Besides, despite no measurable peak shift, we however notice a marked increase in the spectral half-width ($\sim$85 nm as compared to $\sim$65 nm in the reference device) and a significant broadening on the high-energy side. The latter observation, as before, permits one to suspect once again the occurrence of interdiffusion between well and barrier layers, which here is probably limited to a slight blurring of originally abrupt heterointerfaces. On the other hand, the high lasing threshold of this device can be attributed, in addition to defect-induced nonradiative recombination discussed above, to a high optical activity in the damaged region (for example, propagation losses augmented by severe reflections and/or scattering) as discussed below.

Another important characteristic of the damage induced in DBR #2 as deduced from EEL data is shown in Fig. 7. This

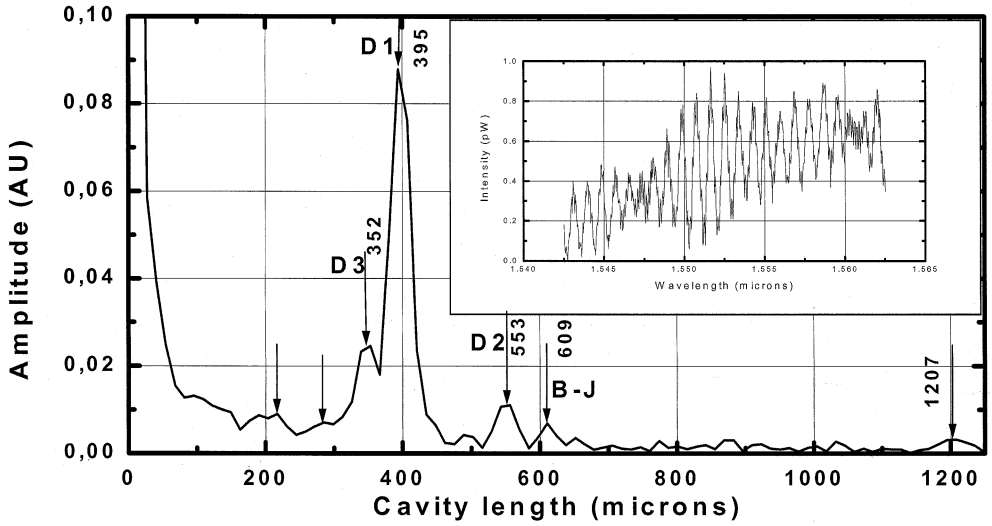

Fig. 7. Graph showing the location of reflection centers (D1, D2, D3, and B-J) in DBR #2 as deduced from FFT treatment applied to a highly resolved EEL spectrum (see inset) recorded at the amplifier end (injection current = 15 mA). Notice the absence of a resonant peak corresponding to the global cavity, suggesting a poor transmission across the device.

graph depicts the results of FFT treatment applied to a highly resolved EEL spectrum (spectral resolution of 0.08 nm compared to 5 nm for all other spectra) presented here as the inset of this figure. One can now remark on the following features of the damaged region that can account for the prominence of reflections in the amplifier section of DBR #2. First, the longest resonant cavity detected in Fig. 7 is located at $\sim$ 609 μm, which precisely corresponds to the location of the butt-joint (B-J) in the device. (Its second harmonic can also be seen at $\sim$ 1207 μm, a distance twice this cavity). Second, there are at least three other independent resonant cavities (labeled here as D1, D2, and D3 in order of increasing amplitudes) that seem to dominate reflections in the amplifier section. Finally and most importantly, the absence of a resonant peak corresponding to the device global cavity (sum of the physical lengths of amplifier and Bragg sections, $\sim$ 1100 μm) confirms once again the poor transmission across this device. The close agreement on the location of principle defects D1, D2, and D3 in the damaged region as deduced from EEL (see Fig. 7) and also the OLCR data [see reflectogram of Fig. 2(b)] is worth noting. As the Bragg section of this device is not affected after burning test (deduced from data of Fig. 3), we conclude that the reflections originating in the amplifier section at the defect centers D1, D2, and D3 severely limit the transmission across this device.

In view of preceding discussions on OLCR mode and EEL mode data, it is obvious that the burning primarily affected the amplifier section of the two tested devices. In DBR #1, the defective region is principally localized close to the exiting end of amplifier section, while in DBR #2, it is found to be located in the neighborhood of the butt-joint and far away from the amplifier end. This explains the poorer quality of EEL spectra recorded from the amplifier end of DBR #1, which evidently are more influenced by a severe nonradiative recombination in the damaged region. On the other hand, in DBR #2, we predicted a higher optical activity (defect-induced reflection and/or scattering) within the damaged region, which is found to contain spatially distributed defects in the neighborhood of the B-J. Also, from the spectral modifications (blue-shift of the peak in DBR #1 and a marked broadening in both DBR #1 and DBR #2 in comparison to the reference device) detected in the EEL spectra, we predicted the occurrence of a partial intermixing between well and barrier layers in the damaged regions of the amplifier sections. Here, we assumed an interdiffusion process, which probably is originated by a significant temperature rise in the device cavity during burning test and/or caused by an abnormally enhanced diffusion promoted by crystalline defects, which are also found to contribute to nonradiative recombination in the damaged region.

IV. Summary and Conclusions

This paper described a first attempt to implement the OLCR and its upgraded facilities to investigate the failure mode of two monolithically integrated two-section DBR lasers on InP that have undergone a burning test under extreme conditions (optical, electrical, and thermal). A fruitful combination of two analytical methods, the OLCR in its conventional reflection mode and its additional in-situ facility in EEL mode, is employed here to investigate the properties of burned devices in comparison to a reference laser. The study revealed several features characteristic of the burning-induced damage. We first employed OLCR in reflection mode to monitor the optical quality of device cavities comprising the Bragg grating. From these experiments, we deduced that the burning alone affected the amplifier (but not the Bragg) section and then spatially localized the damaged regions in each burned device. In the second step, by employing its in-situ EEL mode facility, we further monitored the changes in the optoelectronic quality of the burned devices by recording EEL spectra from either end of the device (amplifier end and Bragg end). In addition to a severe nonradiative recombination and an important defect optical activity, we also noted here significant spectral modifications (blue-shift of the peak and/or an abnormal broadening of the spectral half-width on the high-energy side) in the damaged regions. These results are tentatively

explained by assuming the occurrence of intermixing between the well and barrier layers in the damaged regions of the amplifier section. Considering the low diffusivity of the matrix elements, we predicted a significant rise in temperature spatially localized in the device cavity and/or a defect-enhanced abnormal diffusion during burning test.

In summary, we have shown that a judicious combination of analytical techniques—the conventional OLCR and its additional facilities, as described here—can greatly help to investigate the failure mode of photonic components presently developed on InP for WDM applications. Indeed, such a combination alone provides relevant information on the optical and the optoelectronic qualities of device cavities that otherwise is not accessible with a single analytical method. As shown recently [8], these analytical methods can also be employed as a first step to detect and localize the damaged regions in device reliability studies because of their nondestructive character.

REFERENCES

[1] H. Debrégeas-Sillard, A. Vuong, F. Delorme, J. David, V. Allard, A. Bodéré, O. Gouezigou, F. Gaborit, J. Rotte, M. Goix, V. Voiriot, and J. Jacquet, "DBR module with 20-mW constant coupled output power over 16 nm (40 × 50-GHz spaced channels)," *IEEE Photon. Technol. Lett.*, vol. 13, pp. 4–6, Jan. 2001.

[2] Y. Gottesman, E. V. K. Rao, B. Dagens, and S. Lovisa, "Monitoring of multi-mode imaging devices by use of optical low-coherence reflectometer in reflection and transmission modes," *Appl. Opt.*, vol. 39, pp. 2140–2144, May 2000.

[3] Y. Gottesman, E. V. K. Rao, H. Sillard, and J. Jacquet, "Modeling of optical low-coherence reflectometry recorded Bragg reflectograms : Evidence to a decisive role of Bragg spectral sensitivity," *J. Lightwave Technol.*, vol. 20, pp. 489–493, Mar. 2002.

[4] E. V. K. Rao, Y. Gottesman, and J. G. Provost, "Simple method to diagnose the performance of electroabsorption modulators on InP using optical low-coherence reflectometry," *Appl. Phys. Lett.*, vol. 81, pp. 1552–1554, Aug. 2002.

[5] H. Kressel and J. K. Butler, *Semiconductor Lasers and Heterojunction LED's*. New York: Academic, 1977, pp. 100–102.

[6] E. V. K. Rao, Y. Gottesman, D. Piot, L. Lucatero, E. Vergnol, and M. Pommiès, *Proc. 13th Int. Conf. Indium Phosphide and Related Materials (13th IPRM'01)*, vol. WP-13, Nara, Japan, May 2001, pp. 178–179.

[7] Y. Gottesman, "Exploitation of low-coherence reflectometry to the analysis of photonic components and circuits," Ph.D. dissertation, Univ. of Aix-Marseille III, France, 2001.

[8] Y. Gottesman, M. Pommiès, and E. V. K. Rao, "Detection and localization of degradation damaged regions in 1.3 μm laser diodes on InP using low-coherence reflectometry," *Mater. Sci. Eng.*, vol. B 80, pp. 236–240, 2001.

C. Plouzennec, photograph and biography not available at the time of publication.

Y. Gottesman, photograph and biography not available at the time of publication.

E. V. K. Rao, photograph and biography not available at the time of publication.

H. Sillard, photograph and biography not available at the time of publication.

A. Plais, photograph and biography not available at the time of publication.

J. Jacquet, photograph and biography not available at the time of publication.